Cyanate Dynamics under Algal Blooms and Sediment Resuspension Events in a Shallow Micro-tidal Estuary in the Lower Chesapeake Bay

Yifan Zhu*, Margaret R. Mulholland, Alfonso Macias Tapia, Michael A. Echevarria, Eduardo Perez Vega, Peter Bernhardt

Department of Ocean and Earth Sciences, Old Dominion University, Norfolk, Virginia 23529, United States.

Corresponding author: Yifan Zhu (yzhu003@odu.edu)

Highlights:

- Time series of cyanate concentrations in river system were examined first time
- Cyanate responds rapidly to algal production and wind-induced sediment resuspension
- Cyanate may not be a preferred substrate for nitrifiers in the Lafayette River

Abstract

Although an emerging component in the marine nitrogen (N) cycle, cyanate concentrations and cycling have not been examined in estuarine systems to date. To better understand controls on cyanate concentrations in estuaries, time series data of cyanate and nutrient concentrations in the Lafayette River, a micro-tidal, sub-tributary of the lower Chesapeake Bay, were examined between June and September 2018, and May to September 2019. Cyanate concentrations ranged from near the detection limit (0.4 nmol L^{-1}) to 82.9 nmol L^{-1} in 2018, and 6.8 to 207.4 nmol L^{-1} in 2019. Variations in cyanate concentrations were highly correlated with chlorophyll biomass in the summer, biomass degradation in early fall, and sediment resuspension that occurred in response to meteorological forcing. Cyanate concentrations increased after Chl *a* concentrations decreased suggesting algal decomposition as a source of cyanate. High cyanate concentrations in bottom waters, corresponded to wind-induced sediment resuspension events in the Lafayette River, again suggesting organic matter decomposition as a source of cyanate. Cyanate concentrations in sediment pore water varied between years; in summer 2018, cyanate concentrations were up to 150 nmol L^{-1}, while in 2019, they were three times lower. To confirm an algal source for cyanate, a degradation experiment was conducted using Lafayette River water collected during a bloom of *Margalefidinium polykrikoides* in 2018. In dark incubation bottles, cyanate was one of the first labile organic nitrogen products produced, suggesting the contention that high concentrations of cyanate in late summer and fall were the result of organic matter decomposition. Neither cyanate nor ammonium accumulated in light bottles suggesting production and uptake are tightly coupled and microbes have a high affinity for cyanate in the light. In dark bottles, cyanate production rates were 6.8 nmol L^{-1} d^{-1}, while microbial removal rates during the late phase of degradation were 1.5 nmol L^{-1} d^{-1}, suggesting that cyanate may not be a preferred nitrogen substrate for microbes (including nitrifiers) in dark bottles or that microbes have a lower affinity for cyanate in the dark, allowing cyanate to reach steady state at concentrations greater than the detection limit.

Keywords: Cyanate; cyanate production and regeneration; Lafayette River; *Margalefidinium polykrikoides*; wind-driven sediment resuspension

1 Introduction

Bioavailable dissolved organic nitrogen (DON) compounds (e.g., urea, amino acids, small peptides, and nucleic acids) have been recognized for several decades as nitrogen [N] sources for phytoplankton (Glibert and Legrand, 2006; Bronk et al., 2007; Mulholland and Lomas, 2008). Their availabilities are thought to influence phytoplankton community composition (Berg et al., 2003; Glibert and Burkholder, 2011; Moschonas et al., 2017; Wu et al., 2019) and contribute to algal blooms (Glibert et al., 2001; Mulholland et al., 2002; Davidson et al., 2012; Gobler et al., 2012; Collos et al., 2014). In the spectrum of DON compounds, cyanate has the simplest molecular structure and was only recently discovered to be a source of bioavailable N for phytoplankton (Kamennaya et al., 2008; Hu et al., 2012; Widner et al., 2016). Cyanobacteria, *Prochlorococcus* and *Synechococcus,* were found to encode cyanate hydratase (synonyms - cyanase, cyanate lyase) genes to utilize cyanate (Miller and Espie, 1994; Palenik et al., 2003; Rocap et al., 2003;

Kamennaya et al., 2008; Kamennaya and Post, 2011, 2013) and more recently, it has been demonstrated that cyanate can be assimilated by natural microbial communities (Widner et al., 2016; Widner and Mulholland, 2017; Widner et al., 2018b). While it was initially thought that cyanate was used primarily by prokaryotes, within whose genomes genes for cyanate utilization were first identified, a coastal harmful dinoflagellate species, *Prorocentrum donghaiense*, was cultured using cyanate as its sole source of N (Hu et al., 2012) and a bloom-forming pelagophyte, *Aureococcus anophagefferens*, was also found to possess cyanase genes (Berg et al., 2008) suggesting that cyanate might be more broadly bioavailable. The uptake of cyanate accounted for up to 10% of total measured N uptake in the oligotrophic mid-Atlantic Bight, the Gulf of Maine, and the Eastern Tropical South Pacific Ocean (Widner et al., 2016; Widner and Mulholland, 2017; Widner et al., 2018b), suggesting it is an important but overlooked component of the marine N cycle and that the utilization of cyanate can make a significant impact on N biogeochemistry in coastal and open oceans.

Adding to its emerging recognized biogeochemical significance, cyanate can also be used as a N substrate supporting nitrification (Palatinszky et al., 2015; Kitzinger et al., 2019; Koch et al., 2019; Kitzinger et al., 2020). Some ammonia (e.g., thaumarchaeon *Nitrosopumilus maritimus*, *Nitrososphaera gargensis*, and *Nitrosomonas nitrosa*) and nitrite oxidizing microbes (e.g., *Nitrospira moscoviensis* and *Nitrospinae bacteria*) mediated the conversion of cyanate to either ammonium or nitrite, both directly and indirectly, even though cyanate hydratase genes were not identified in all of these organisms in genomic analyses (Palatinszky et al., 2015; Kitzinger et al., 2019; Kitzinger et al., 2020). Cyanate can also be a primary substrate for anaerobic ammonium oxidation (anammox), a process recently dubbed "cyanammox", in oxygen deficient zones, such as those that occur in the Eastern Tropical Pacific Ocean (Babbin et al., 2017; Widner et al., 2018a). In the Eastern Tropical North Pacific Ocean, the contribution of cyanate to anammox was equivalent to ammonium at the top of the oxygen deficient zone (Babbin et al., 2017), and cyanate lyase genes were present at all depths sampled, where *Nitrospina* and *Scalindua* were located (Widner et al., 2018a). Together, these observations suggest that cyanate, like ammonium, is a central and dynamic component of the N cycle despite its low environmental concentrations.

Similar to other reactive DON species such as urea, amino acids, and small peptides, cyanate was shown to be produced during cellular metabolism (e.g., by intracellular urea and/or carbamoyl phosphate breakdown) (Kamennaya et al., 2008; Kamennaya and Post, 2011), and extracellularly as a result of photochemical reactions and during degradation of algal cultures at rates comparable those of other labile nitrogen compounds such as ammonium and amino acids (Widner et al., 2016). Because its production and consumption appear to be tightly coupled, as for other N cycle intermediates such as ammonium and nitrite, cyanate seldom accumulates in the water column or soils, with concentrations typically observed at nanomolar levels in most environments examined to date (Mooshammer et al., 2021). As for ammonium and nitrite, vertical profiles of the water column typically show subsurface cyanate maxima just below the chlorophyll maximum, reflecting biological consumption in surface waters, production in subsurface waters where regeneration is substantial, and depletion in deep waters as reduced N is oxidized (Widner et al., 2016; Widner and Mulholland, 2017). Spatially, cyanate concentrations are generally highest in coastal/shelf waters where productivity and terrestrial inputs of organic matter are higher and decrease with distance from the land (Widner et al., 2016; Widner and Mulholland, 2017). For example, cyanate concentrations near the Chesapeake Bay Mouth were <40 nmol L^{-1} (Widner et

al., 2013), decreased to <10 or 20 nmol L^{-1} in mid-Atlantic Bight and Gulf of Maine (Widner and Mulholland, 2017), and were <5 nmol L^{-1} in oligotrophic waters influenced by Gulf Stream (Widner et al., 2016). From the limited measurements available, cyanate-N concentrations were ~5% - 30% of ammonium-N concentrations in continental shelf waters (Supplementary Fig. 1 from Kitzinger et al., 2019).

Previous studies of cyanate utilization by phytoplankton were focused primarily on prokaryotic phytoplankton that occurs in oceanic regimes and is known to have and express cyanate hydratase genes (e.g., *Prochlorococcus* and *Synechococcus*) (Palenik et al., 2003; Kamennaya et al., 2008; Kamennaya and Post, 2011). However, recent studies conducted in coastal waters in the North Atlantic Ocean between Cape Hatteras and the Gulf of Maine suggest that a broader group of eukaryotic phytoplankton may utilize cyanate to support their growth and that cyanate production may be dependent on the availability of labile organic matter (Widner and Mulholland, 2017). Estuaries such as the Chesapeake Bay are dominated by eukaryotic phytoplankton, mainly diatoms and dinoflagellates (Harding et al., 2015), tend to be meso- or eutrophic, and have ambient DON, dissolved inorganic nitrogen (DIN), and phytoplankton concentrations up to three orders magnitude higher than those observed in coastal and oceanic systems (Harding et al., 2016; Testa et al., 2018; Harding et al., 2019). These systems are also prone to substantial terrestrial inputs of DIN and DON through runoff (Austin, 2002; Hagy et al., 2004; Zhang et al., 2015), which may provide potential direct and indirect sources of cyanate. Based on this, we hypothesized that cyanate production rates were likely to be high in estuarine systems. In addition to water column processes, sediments accumulate organic matter in shallow eutrophic estuaries, and remineralization of sedimentary organic N can play an important role in N biogeochemistry in these systems (Cowan and Boynton, 1996; Burdige and Zheng, 1998), thus, sediment might be a potential source of cyanate.

The Lafayette River is a shallow, eutrophic, micro-tidal sub-tributary of the lower Chesapeake Bay (Fig. S1, supporting information), prone to recurring harmful algal blooms (HABs). Over recent decades, seasonal dinoflagellate blooms, including nearly annual summer blooms dominated by *Margalefidinium polykrikoides* (*M. polykrikoides*), have been observed in this system resulting in chlorophyll a (Chl *a*) concentrations of > 200 μg L^{-1} (Mulholland et al., 2009; Morse et al., 2011; Egerton et al., 2014; Hofmann et al., 2021). Because the Lafayette River was identified as a site where blooms initiated (Morse et al., 2013), a time series site was established there in 2012. Ambient DIN concentrations in the Lafayette River are often >10 μmol L^{-1}, DON concentrations >20 μmol N L^{-1}, and concentrations of dissolved inorganic phosphorus (DIP, refers to phosphate [PO_4^{3-}]) typically range from 2–9 μmol P L^{-1} μmol L^{-1} (Morse et al., 2014). However, during summertime blooms, DIN concentrations are typically at the limit of analytical detection, and DON concentrations drop to as low as 13 μmol N L^{-1} (Mulholland et al., 2009; Morse et al., 2014). In the summer, there are interspersed periods of stratification and event-scale processes, including tropical storms, that mix the water column and re-suspend sediments thereby modulating benthic-pelagic coupling. Wind-driven sediment resuspension can inject nutrients regenerated from sedimentary organic matter decomposition into the water column (Morse et al., 2011; McGill et al., 2019). The unique environmental setting of the Lafayette River and the availability of time series data make this an ideal system to investigate how intense algal production, biomass, and sediment resuspension affect the biogeochemical cycling of cyanate in estuarine environments. To advance our understanding of cyanate within the estuarine N cycle, we

examined the distribution of cyanate in the water column and sediments of the Lafayette River and here we provided a time series of cyanate concentrations relative to those of Chl *a* and other dissolved N species over two contrasting summers; one during which there was an intense *M. polykrikoides* bloom where Chl *a* concentrations reached upwards of 400–500 μg L^{-1} (2018), the other when there was no bloom (2019).

2 Materials and Methods

2.1 Sensor deployment

Water quality sondes (Model 6600, Yellow Spring International [YSI], Inc., USA) were deployed near the surface at two fixed stations in the Lafayette River, Virginia, from May 1 to September 30 in 2018 and 2019; one was located at Norfolk Yacht and Country Club near the mouth of the river where the maximum water depth was approximately 6 m (NYCC, [36.91°N, -76.30°E]); and the other was near the headwaters of the river, where the maximum water depth was approximately 2 m (AC, [36.88°N, -76.27°E]) (Fig. S1, supporting information). YSI sondes were equipped with sensors to measure pressure (a proxy of water depth), temperature, conductivity (a proxy of salinity), pH, chlorophyll fluorescence (a proxy for Chl *a* concentration), dissolved oxygen (DO), and turbidity. The sampling frequency of the moored sondes was every 15 mins in unattended sampling mode. Sondes were exchanged every 1–2 weeks for cleaning and calibration. After retrieval, data was downloaded, and sensors were calibrated according to the manufacturer's specifications and protocols established by Hampton Roads Sanitation District as part of their routine water quality monitoring in accordance with their US Environmental Protection Agency (EPA) discharge permit. Chlorophyll fluorescence data was corrected using the daily extracted chlorophyll data (see below). Conductivity data were converted to practical salinity (S_P, unitless) and then to absolute salinity (S_A, g kg^{-1}) based on the current TEOS-10 standard (Martins and Cross, 2022).

In addition to data from the surface moored sondes, vertical profiles were collected almost daily, at both sites, using identical instruments near mid-day, when solar radiation is predicted to be at its peak, to examine hydrographic parameters over the water column. The sampling frequency was rapid (seconds) under discrete sampling mode. On average, the YSI sonde collected data at every 0.1–0.2 m interval during the vertical profiling. Because *M. polykrikoides* vertically migrate on a daily schedule (Park et al., 2001), the timing of sampling was intended to coincide with the time of day when Chl *a* was concentrated in surface waters. In 2018, daily vertical sonde deployments were conducted at AC from June 1 until July 31 when a bloom of *M. polykrikoides* was first detected (>1,000 cells mL^{-1}). Subsequently, daily vertical profiling was moved to our down-estuary site at NYCC where high Chl *a* concentrations persisted from August 1 to September 30. In 2019, vertical deployments of YSI sondes were conducted daily at both sites from May 1 to September 30. Sondes used for vertical profiling were cleaned and calibrated as described above. While ideally sampling would have been congruent during both years, this study leveraged ongoing projects. Data and quality assurance and quality control protocols are publicly available on the Virginia Estuarine and Coastal Observing System (VECOS) website hosted by the Virginia Institute of Marine Science (http://vecos.vims.edu).

2.3 Water column and pore water sampling.

Water column sampling was conducted alongside the vertical profile data collections described above. Samples to measure cyanate, ammonium (NH_4^+), urea, nitrate (NO_3^-), nitrite (NO_2^-), and PO_4^{3-} concentrations were pumped from three depths (near-surface, an intermediate water depth, and near-bottom) at each site through a 0.2 μm Polycap TC encapsulated filter (Whatman®) affixed to a portable peristaltic pump system (Masterflex E/S, Cole-Parmer, USA). Since the water level changes with tide (e.g., varying 4.8–6.1 m at site NYCC, see Fig. S2, supporting information), the three sampling depths varied as well: 0.5 (or 0.25), 2.5, and 4.25 m during low tides, 0.5 (or 0.25), 3, and 5 m during intermediate tides, and 0.5 (or 0.25), 3, and 5.75 m during high tides. Similarly, at site AC, the water depth varied from 1.2–2.2 m, so the three sampling depths were targeted at 0.25 (or 0.5), 0.75, and 1 m when it was low tide, 0.25 (or 0.5), 1, and 1.5 m at intermediate tides, and 0.25 (or 0.5), 1.25, and 2 m when it was high tide. Samples for NH_4^+ (in triplicate), NO_3^-, NO_2^-, urea, and PO_4^{3-} analyses were filtered on site and collected directly into sterile polypropylene centrifuge tubes (Falcon®). Cyanate samples were placed into 1.8 ml sterile microcentrifuge tubes with O-ring seals (Micrewtube®). Samples were stored and transported in a cooler with ice packs and returned to the laboratory within 2 hours of their collection (usually less). In the laboratory, nutrient samples were immediately frozen upright at -20°C and cyanate samples were immediately stored at -80 °C until analysis. In addition to filtered samples, whole water samples for identifying and numerating *M. polykrikoides* and other taxonomic phytoplankton groups were preserved with iodine Lugol's solution at the time of collection. Whole water was also pumped into dark high-density polyethylene (HDPE) bottles (Nalgene®) and stored in a cooler and then transported to the laboratory. Immediately upon arrival, these water samples were mixed, and sub-samples were collected onto pre-combusted glass fiber filters (GF75, Whatman®, nominal pore size 0.3 μm) in triplicate for analysis of Chl *a* concentrations to provide biomass estimates and correct the YSI fluorescence data. These filters were stored frozen until analysis within two weeks of their collection.

Sediment cores were collected at AC using a cylindrical gravity corer to examine the potential cyanate production from organic matter degradation in the sediments in summer 2018 and 2019. In July 2018, samples were collected by slicing sediment cores into three layers (0–3 cm, 3–6 cm, and 6–9 cm). Sliced sediments were then centrifuged, and the resulting pore water (supernatant) was syringe-filtered through GF75 filters and frozen (-80 ℃) until analysis. In 2019, three sediment cores were collected, two from August 20, the other one from August 27. For each sediment core, pore water samples (~1.8 ml) were withdrawn, through holes drilled at 2 cm increments (0, 2, 4, 6, 10 cm) in the polycarbonate core sleeve, using a syringe and then filtered through GF75 (nominal pore size of 0.3 mm) filters. Filtrate was frozen for cyanate analysis as described above.

2.4 Algal degradation experiments

During 2018, there was a massive *M. polykrikoides* bloom while in 2019 there was not. In August 2018, a 50-day incubation experiment was conducted to examine the production of cyanate and other nitrogenous nutrients during degradation of natural microbial community assemblages using natural estuarine waters collected during a bloom of the dinoflagellate, *M. polykrikoides*. Surface water was collected within the *M. polykrikoides* bloom when Chl *a* concentrations were

extremely high (105 μg L^{-1}) using a clean bucket and then gently transferred to a 20 L carboy and transported back to the laboratory where an acid-cleaned Teflon magnet was added, and the carboy was placed on a stir-plate to keep the microbial community homogenized. Water from the carboy was dispensed into triplicate, dark HDPE bottles (2 L) and triplicate, clear polycarbonate bottles (2 L). All bottles were placed in an illuminated incubator (Precision Scientific, USA) set at 27 °C (near ambient water temperatures) supplied with a 14:10 h light:dark cycle with a light intensity of 700 μE m^{-2} s^{-1} for 50 days. Samples were collected from incubation bottles and filtered through GF75 filters to measure the production of dissolved constituents, including cyanate, urea, NH_4^+, NO_2^-, NO_3^-, and PO_4^{3-} at days 0 (the start of the experiment), 1, 3, 4, 6, 7, 10, 14, 19, 22, 26, 29, 33, 37, and 50. Samples were frozen until their analysis as described below. Since there was no *M. polykrikoides* bloom in 2019, no degradation experiments were undertaken in that year.

2.5 Sample analyses

Cyanate concentrations were measured using a pre-column fluorescence derivatization method and high-performance liquid chromatography (Widner et al., 2013; Widner and Mulholland, 2017). The method detection limit (MDL) was 0.4 nmol L^{-1} (Widner et al., 2013). Micromolar concentrations of NO_3^-, NO_2^-, PO_4^{3-}, and urea were determined using a nutrient autoanalyzer according to the manufacturer's specifications (Astoria-Pacific, Inc., USA); NO_3^- + NO_2^- (N+N) samples were analyzed using the standard azo dye colorimetric method (Whitledge et al., 1981). PO_4^{3-} was determined using the phosphomolybdenum blue (PMB) method (Bernhardt and Wilhelms, 1967). Urea concentrations were measured by the diacetyl monoxime method (Rahmatullah and Boyde, 1980). The MDLs for N+N, PO_4^{3-}, and urea were 0.14 μmol L^{-1}, 0.03 μmol L^{-1}, and 0.08 μmol L^{-1}, respectively. NH_4^+ concentrations were analyzed manually using the manual indophenol method with the MDL of 0.02 μmol L^{-1} (Strickland and Parsons, 1972). Both NH_4^+ and Chl *a* samples were analyzed within 10 days of their collection. To measure extracted Chl *a* samples, the frozen filters were submerged in 10 mL 90% acetone and extracted in a freezer (-20°C) for 24 hrs. before measuring fluorescence on a 10-AU Turner Fluorometer (Welschmeyer, 1994). Major taxonomic phytoplankton group identification and algal cell enumeration were carried out using an inverted microscope (100–600×, model CKX41, Olympus, Japan). Cell densities were reported as cells mL^{-1}. *M. polykrikoides* blooms have been defined as when their cell abundance exceeds 1000 cells mL^{-1} (Marshall and Egerton, 2009).

2.6 Data analysis

Data collected from YSI vertical profiles were binned at 0.1 m and 0.25 m intervals for AC and NYCC, respectively. Water column density gradients were calculated from vertical profile data to assess the degree of stratification such that density (ρ_w) differences were calculated over discrete depths (z) in the water column using Eq.1, without filtering the effect of tidal and wind straining. z was 0.1 m and 0.25 m interval for AC and NYCC, respectively. For *n* number of measurements referenced from the surface, for $i = 1$ to $i = n - 1$:

$$Density\ gradient = \frac{\partial \rho_w}{\partial z} = \frac{\rho_{i+1} - \rho_i}{z_{i+1} - z_i} \qquad (1)$$

Therefore, the more stratified the water column the more positive the value of the density gradient. In this case, the water column was deemed stratified when the density gradient was higher than 0.5 kg m^{-4}.

Hourly wind and precipitation data at Norfolk Naval Station (station ID: 13750, [36.95°N, -76.30°E]) were downloaded from https://www.ncdc.noaa.gov/cdo-web/datatools/lcd. A one tailed *t*-test was applied to examine if daily average windspeed was correlated to bottom water DIN and cyanate concentrations. In addition, the cross-correlation tool in MATLAB (R2021b, MathWorks) was used to examine the relationship between daily average windspeed (n=61) and daily bottom water DIN and cyanate concentrations, during August-September 2018. The DIN and cyanate data contained missing values (19 out of 61) and interpolating the data could make the data points more continuous (fill data gaps). Thus, data gaps were filled by running a "spline" model. However, for the same period of 2019, the measured nutrient data points (n= 21, out of 61) were not sufficient, filling the data gaps brought poor and misleading results (data not shown here), therefore, cross-correlation was only performed for August-September 2018.

3 Results

3.1 Environmental parameters from surface mooring data and vertical profile data

Water temperatures were generally higher at AC and more variable than at NYCC throughout the summer (see Figs. 1a and 1d, and 3a and 3g), due to its shallower depth. Surface water temperatures at AC varied from 24.6 to 33.5 °C with the average of 28.9 ± 1.7 °C between June-September 2018 (Fig. 1a), and 20.3 to 34.4 °C with the mean value of 27.7 ± 2.3 °C in the same period of 2019 (Fig. 1a). Surface water temperatures at NYCC ranged 23.8–31.6 °C with the mean of 27.9 ± 1.4 °C between June-September 2018 (Fig. 1d), and 22.7–32.6 °C with the mean of 26.8 ± 1.8 °C in the same period of 2019 (Fig. 1d). In general, water temperatures at AC and NYCC were greater during July and August and then decreased in late September, although sporadic cooling was observed with the passage of storms (Figs. 2a and 2g, 3a and 3g).

Overall, surface salinities appeared to gradually increase over the summer in both years and were higher by ~ 3–4 in 2019 than that of 2018 for both sites (Figs. 1b and 1e, 2b and 3b, and 2h and 3h), although there were large data gaps at AC in 2018 due to a sensor failure. Salinity at AC (Figs. 2b and 3b) was slightly lower than that at NYCC (Figs. 2h and 3h) in both years, not surprising since the AC station is nearer the headwaters and NYCC near the mouth of the estuary. Briefly, surface water salinity at AC ranged 12.2–19.5 with the mean of 16.3 ± 1.8 during June-September 2018 (Fig. 1b), and 7.8–23.5 with the average of 17.9 ± 3.2 in the same period of 2019 (Fig. 1b). Surface salinity at NYCC varied 13.8–22.8 with the average of 18.5 ± 2.1 during June-September 2018 (Fig. 1e), and 15.0–27.5 with the average of 21.5 ± 3.2 in the same period of 2019 (Fig. 1e). During both years salinities were within the ranges reported from the Chesapeake Bay Program monitoring data (https://datahub.chesapeakebay.net). Both temperature and salinity determine water column stratification and were periodically affected by weather events such as storms and precipitation. At AC, the water column was periodically stratified in June and consistently stratified in July of both years and in August 2019 (Figs. 2c and 3c). Water column stratification at NYCC was common in August in both 2018 and 2019 (Figs. 2i and 3i) with periodic stratification in June and July 2019 (Fig. 3i). The periods when the water column was

stratified coincided with periods of high Chl *a*, at AC in July 2018 (Fig. 2c and 2d) and July-September 2019 (Fig. 3c and 3d), and at NYCC in August 2018, when two algal blooms occurred (Fig. 2i and 2j).

Chl *a* concentrations at AC were higher in June and late July (over 100 μg L^{-1}) during 2018 when a bloom of *M. polykrikoides* initiated than during the same period in 2019 (Fig. S3, a & c, supporting information), however, Chl *a* concentrations were sporadically high at AC throughout August and September during both years (Fig. 1c, 2d, and 4e). While Chl *a* concentrations at AC were sometimes high in 2019, especially in July and throughout August (Figs. 3d and 5e) when the phytoplankton community was dominated by another dinoflagellate (Fig. S3, c & e, supporting information), there was no *M. polykrikoides* bloom during that year. Chl *a* concentrations at NYCC were generally less than 30 μg L^{-1} until the end of July 2018 (Fig. 1f). Throughout August 2018, high Chl *a* concentrations (over 100 μg L^{-1}) were observed at NYCC where a bloom of *M. polykrikoides* occurred (Fig. 1f). Sometimes Chl *a* concentrations reached the maximum capacity of the fluorescence sensor (400–500 μg L^{-1}, Figs. 2j and 4j) when *M. polykrikoides* concentrations reached >25,000 cells mL^{-1} (Fig. S3b, supporting information). After the bloom dissipated, Chl *a* concentrations decreased to 5–20 μg L^{-1} in mid-September (Figs. 1f and 2j). In contrast, Chl *a* concentrations seldom exceeded 30 μg L^{-1} at NYCC throughout the summer in 2019 when there was no bloom (Figs. 1f, 3j, and 5j). DO concentrations were mostly greater than 4 mg L^{-1} (saturation > 50%), showing the Lafayette River was well oxygenated (Figs. 2e & k and 3e & k). DO hotspots were correlated with high Chl *a* concentrations (Figs. 2d-e, 2j-k, and 3d-e). Turbidity at AC (Figs. 2f and 3f) was much higher than at NYCC (Figs. 2l and 3l) in both years due to the shallower water depth, sediment resuspension events, and higher Chl *a* (McGill et al., 2019). In July 2018 and July-August 2019, turbidity at AC was notably higher than in other months (Figs. 2f and 3f). Some of this was likely due to high Chl *a* concentrations. At NYCC, turbidity was generally higher near the bottom but sporadically high throughout the water column when storms passed through (Figs. 2l and 3l) with winds sufficient to cause sediment resuspension. In section 3.4, the relationship between wind-induced sediment resuspension and bottom nutrients at NYCC is reported.

3.2 Cyanate and nutrient concentrations in the Lafayette River

In 2018, cyanate concentrations ranged from near the detection limit to 82.9 nmol L^{-1}, with the highest concentrations observed in late summer (Fig. 4a & f). At AC, cyanate concentrations were high in June and again in late July (Fig. 4a). At NYCC, cyanate concentrations reached 81.7 nmol L^{-1} on August 2, as the *M. polykrikoides* bloom was initiating (Fig. 4f). Subsequently, cyanate concentrations remained at or below 30 nmol L^{-1} until mid-September when cyanate concentrations reached 82.9 nmol L^{-1} (Fig. 4f). Similar to cyanate concentrations, NH_4^+ concentrations were high at AC in early and mid-June, ranging 2.2–5.5 μmol L^{-1} (Fig. 4b), increasing to 12.5 μmol L^{-1} on June 20 after a storm (storm 1, Fig. 4b). Concentrations were below the limit of analytical detection at AC throughout most of July except in late July when there was another storm (storm 2, Fig. 4b) and NH_4^+ concentrations up to 15.9 μmol L^{-1} were observed. NH_4^+ concentrations at NYCC were generally at or near the limit of analytical detection throughout the summer except for a few episodically high concentrations during August, associated with the passage of storms (e.g., storms 3 and 4, Fig. 4g) and high turbidity (Fig. 2l). NH_4^+ concentrations increased after the *M. polykrikoides* bloom terminated with concentrations up to 4.0 μmol L^{-1}

observed in early September, which was also coincident with a tropical storm (storm 5, Fig. 4g). As for NH_4^+, N+N concentrations were mostly undetectable throughout the summer with a few exceptions linked with the passage of storms and associated rainfall (Figs. 4c and 4h). N+N concentrations increased by an order of magnitude in September 2018 after the *M. polykrikoides* bloom terminated, reaching concentrations as high as 35.8 μmol L^{-1} (Fig. 4h). Concentrations of PO_4^{3-} were never depleted over the sampling period, ranging 2.8–6.1 μmol L^{-1} (Figs. 4d and 4i), and were generally lower after mid-July, dipping during the period when *M. polykrikoides* abundance was highest between August 16–21, when PO_4^{3-} was drawn down to 0.6 μmol L^{-1} (Fig. 4i).

In 2019, dissolved cyanate, NH_4^+, and N+N concentrations at AC were generally lower than in 2018 between May and August (Figs. 5a-c and 4a-c, respectively). Concentrations of cyanate, NH_4^+, and N+N were markedly higher at NYCC than AC during May (Figs. 5f-h and 5a-c, respectively). Overall, concentrations of all 3 analytes were depleted throughout much of the rest of the summer excluding periods when storms passed through and may have introduced nutrients through runoff and resuspension of sediments. Cyanate concentrations reached 207.4 nmol L^{-1} in May at NYCC (Figs. 5f) and exceeded 100 nmol L^{-1} in September at both NYCC and AC (Figs. 5a and 5f). At both sites, cyanate concentrations were usually <50 nmol L^{-1} during most of the period between June and August (Figs. 5a and 5f). Like cyanate, NH_4^+ concentrations at AC were mostly undetectable throughout the summer in 2019, only occasionally increasing in association with summer storm or wind events during July and August (Fig. 5b). NH_4^+ concentrations at NYCC (Fig. 5g) were low but fluctuated throughout the summer and were highest at both sites at the end of the summer, reaching 6.8 μmol L^{-1} (Figs. 5b and 5g). Urea concentrations were undetectable for most of the sampling period at both sites (Figs. 5b and 5g). Concentrations of N+N at NYCC in 2019 (Fig. 5h) were generally much lower than those observed in 2018 (Fig. 4h), ranging from near the analytical detection limit throughout most of the summer, to 9.5 μmol L^{-1} during the early fall (Fig. 5h). Similar to NH_4^+ and cyanate, N+N concentrations at AC and NYCC (Figs. 5c and 5h) were higher in both early May and late September and were at or near the analytical detection limit during the summer except for sporadic increases associated with the passage of storms in mid-June and early August. The late summer N+N maxima at AC (Fig. 5c) was much lower than that observed at NYCC (Fig. 5h). PO_4^{3-} concentrations at AC ranged 1.5–6.9 μmol L^{-1} with an average concentration of 3.6 ± 1.3 μmol L^{-1} (Fig. 5d), slightly higher than that at NYCC (Fig. 5i), where PO_4^{3-} concentrations varied 0.3–6.2 μmol L^{-1} with the mean concentration of 2.7 ± 1.2 μmol L^{-1} and generally increased over the course of the summer.

3.3 Influence of wind-induced sediment processes on bottom cyanate and DIN variations

During the sampling period, the wind most commonly came from the WSW and was associated with low speeds (<5 m/s). The most intense winds blew from the NNE and reached >7.5 m/s during August-September (Fig. S4, supporting information). The relationship between wind speed and direction, precipitation, and bottom water cyanate and DIN (the sum of NH_4^+ and N+N) concentrations in August and September 2018 and 2019, were examined (Fig. 6) to determine whether wind- or storm-induced sediment resuspension events may have released cyanate and other nitrogenous nutrients to the water column. Between August 1 and August 4, 2018, precipitation associated with high south/southwesterly winds with speeds >5 m s^{-1} (Fig. 6a), defined here as a storm event (storm 3, Fig. 4), were aligned with high bottom water DIN and

cyanate concentrations (Fig. 6b). These high concentrations of nitrogen compounds were rapidly depleted, with concentrations returning to undetectable levels on August 6 (Fig. 6b). Furthermore, elevated nutrient concentrations in bottom waters appear not only associated with wind speed, but also with wind direction. For example, during August 30–31, 2018, southerly wind abruptly switched to northerly wind (storm 4, Figs 4 and 6a), resulting in elevated bottom DIN and cyanate concentrations (Figs. 4f-h and 6b). Notably, hurricane Florence impacted Norfolk from September 12 to 16, 2018 (storm 5, Fig. 4), during which time northeasterly winds exceeded 10 m s^{-1} (Fig. 6a), causing huge nutrient releases from sediments into bottom waters (Fig. 6b). During and just after this event, bottom cyanate and DIN concentrations increased by a factor of 3 to 4 (Fig. 6b). Similar to 2018, in summer 2019, storm 3 (August 22–28), storm 4 (hurricane Dorian, September 5–6), and storm 5 (September 13–14) (Fig. 6c) resulted in high bottom water concentrations of cyanate and DIN (Fig. 6d).

3.4 Sediment pore water concentrations

Cyanate concentrations in sediment pore water profiles exhibited distinct variations between years (Fig. 7). In July 2018, cyanate concentrations in pore waters ranged from 120 to 150 nmol L^{-1}, increasing slightly with depth (Fig. 7). The concentrations in the sediment were a few times higher than those in the water column at the same time (Fig. 4a). In contrast, in August 2019, cyanate concentrations were three times lower than in 2018, ranging 0.4–67.8 nmol L^{-1}, and generally decreased with depth, these concentrations were similar to those observed in the water column at the same time (Fig. 5a).

3.5 Phyto-detritus decay experiments

Incubations of natural water samples collected during blooms were conducted in 2018 to determine whether cyanate was produced during phytoplankton degradation in the environment. In dark bottles, we observed the sequential production of NH_4^+, NO_2^-, and NO_3^- (Fig. 8a), as has been observed previously (Sima et al., 2020), however, along with NH_4^+, we also observed that cyanate and urea were released as primary degradation products (Figs. 8b and 8c, respectively). Concentrations of NH_4^+, cyanate, and urea increased rapidly over the first 2 days of our degradation experiments, reaching their concentration maxima nearly simultaneously after 10–15 days of incubation (Figs. 8a-c). The concentration maxima were 26.9 μmol L^{-1} for NH_4^+ (Fig. 8a), 70.7 nmol L^{-1} for cyanate (Fig. 8b), and 2.0 μmol L^{-1} for urea (Fig. 8c). Production of these reduced intermediate compounds was followed by a production of NO_2^-, another N cycle intermediate, that reached its maximum concentration of 36.5 μmol L^{-1} after 22 days (Fig. 8a). Ultimately, NO_2^- was nitrified to NO_3^-, which reached concentrations of 40 μmol L^{-1} after 37 days and completing the nitrification process (Fig. 8a). Notably, urea was consumed rapidly after reaching its maximum (Fig. 8c) while cyanate was not (Fig. 8b). Concentrations of PO_4^{3-} increased from ~3 μmol L^{-1} to ~6.7 μmol L^{-1} after about 15 days (Fig. 8d). In contrast, in light bottle incubations, the concentrations of all the nitrogenous compounds measured remained near or at the analytical detection limits for the duration of incubation experiment suggesting a tight coupling between their production and consumption (Figs. 8a-c). Concentrations of PO_4^{3-} remained 2–4 μmol L^{-1} throughout most of the light incubation experiments and then decreased to ~0.6 μmol L^{-1} at the end of the incubation (Fig. 8d). Detailed concentrations of N and phosphate are shown in table S1 and S2 in supplementary materials.

4 Discussion

4.1 Cyanate cycling in the Lafayette River

This study shows that cyanate concentrations in the Lafayette River are an order of magnitude higher (up to 207 nmol L^{-1}) than those observed in the North Atlantic continental shelves and slope sea (Widner et al., 2016; Widner and Mulholland, 2017), the Gulf of Mexico shelf waters (Kitzinger et al., 2019; Kitzinger et al., 2020), and the Eastern Tropical Pacific (Widner et al., 2018a; Widner et al., 2018b). This is not surprising given the relationships previously observed between Chl *a* and cyanate concentrations. As for these other systems, cyanate variations in the Lafayette River appears to be regulated by primary productivity and the production of organic matter. Specifically, cyanate and other N compounds (e.g., NH_4^+) were generally depleted in summer when algal productivity and biomass were highest (Figs. 4a-c, 4f-h 5a-c, and 5f-h). High cyanate concentrations in late spring (see Fig. 5f), likely reflect the accumulation of reduced N cycle intermediates due to lower consumption by phytoplankton. Higher concentrations in fall after the period of maximum chlorophyll biomass are likely due to decomposition of phytoplankton and nitrification of organic matter and reduced N compounds. As revealed from the Phyto-detritus decay experiment (Figs. 8a-d), calculated DIN:DIP was ~10, however, the measured DIN:DIP in the Lafayette River during the period before the bloom in 2018 was <1, indicating that the phytoplankton community in general was N-limited, potentially using organic nitrogen to support their N demand. Indeed, *M. polykrikoides* is a known mixotroph and like other dinoflagellates that bloom in the lower Chesapeake Bay (e.g., *Gymnodinium* spp., *Akashiwo sanguinea*, and *Prorcentrum minimum*), can take up organic nutrients, including urea and amino acids, and hydrolyze small peptides (Mulholland et al., 2009; Tang et al., 2017; Mulholland et al., 2018). Gobler et al. (2012) similarly found that blooms of *M. polykrikoides* often occurred when concentrations of DIN were <2 μmol L^{-1} and DON >20 μmol L^{-1} in New York estuaries. It is noted that even in spring and fall (September), when cyanate was most abundant, its concentrations were 2–3 orders of magnitude lower than those of other measured N sources. At this point, the contribution of cyanate to the N demand during blooms in the Lafayette River is unclear. While cyanate uptake was not measured in this study, a variety of phototrophic cyanobacteria and eukaryotes (e.g., *Prochlorococcus*, *Synechococcus,* and *Prorocentrum donghaiense*) are known to take up cyanate to meet their N demand (Kamennaya et al., 2008; Hu et al., 2012; Kamennaya and Post, 2013; Widner and Mulholland, 2017). Metatranscriptomics profiling strikingly reveals that dinoflagellate species, *Alexandrium fundyense*, has the versatility to exploit various source of organic N compounds, e.g., cyanate, urea, under nitrate depleted condition (Zhuang et al., 2015; Elferink et al., 2020).

Here, we demonstrate that cyanate, along with other reduced N compounds and N cycle intermediates, e.g., NH_4^+ and urea, were the first degradation products released during algal decomposition (Figs. 8a-c). While NH_4^+ and urea were subsequently oxidized in our experimental incubations (Figs. 8a and 8c, respectively), cyanate did not appear to be removed/nitrified (Fig. 8b). Kitzinger et al. (2019) discovered that cyanate can be directly used as both energy and N sources by ammonia-oxidizing archaea (*Nitrosopumilus maritimus*) in the hypoxic shelf waters of Gulf of Mexico, likely through extracellular breakdown to NH_4^+, since this organism did not contain cyanase. Some bacterial nitrite oxidizers in the same area, e.g., *Nitrospinae*, were also found capable of incorporating N from cyanate despite observations that cyanase was rarely

detected (Kitzinger et al., 2020). While other nitrite oxidizers, e.g., *Nitrospira moscoviensis*, *Nitrospina gracilis*, *Nitrospira marina*, and anammox/cyanammox bacteria (e.g., *Candidatus* Scalindua), were found to possess cyanase-encoding genes to facilitate cyanate utilization (Lücker et al., 2010; Palatinszky et al., 2015; Babbin et al., 2017; Pachiadaki et al., 2017; Ganesh et al., 2018; Widner et al., 2018a; Bayer et al., 2021), the mechanism by which cyanate is being mobilized by cyanase-deficient microbes remains unclear. It was suggested that cyanase-negative ammonia oxidizers and cyanase-positive nitrite oxidizers may have developed reciprocal/cross-feeding strategies that benefit both microorganisms when they co-aggregate (Palatinszky et al., 2015; Pachiadaki et al., 2017).

This study showed that the net rate of cyanate production during degradation of natural phytoplankton assemblages was ~6.8 nmol L^{-1} d^{-1} during the linear portion of the decay process (first 10 days, Fig. 8b), in agreement with the production rates of 5–9 nmol L^{-1} d^{-1} observed previously in diatom cultures (Widner et al., 2016). However, the net removal rate of cyanate during the late phase of degradation in dark incubations was only ~1.5 nmol L^{-1} d^{-1}, much slower than the measured rate of ~10–54 nmol L^{-1} d^{-1} observed in hypoxic/anoxic shelf waters of the Gulf of Mexico (Kitzinger et al., 2019) and 33.4 ± 48 nmol L^{-1} d^{-1} in the Eastern Tropical North Pacific oxygen deficient zone (Widner et al., 2018b) from ^{15}N-cyanate addition incubations. This suggests that microbial nitrifier communities in the lower well-oxygenated Chesapeake Bay may have different physiological capabilities (e.g., lower affinity for cyanate) than those residing near or within oxygen deficient water. Not all nitrifiers possess cyanate encoding genes that enable cyanate utilization (Pachiadaki et al., 2017), thus we cannot rule out the possibility that the slow removal rate of cyanate may simply reflect the inability of resident nitrifiers to use cyanate, and thus it indicates a slow abiotic decay process of cyanate. We also realized that the actual turnover rates of cyanate were not measured, and inferences made based on N concentrations alone may be inconclusive if production and consumption are balanced. Steady state nutrient concentrations reflect a balance between production and consumption and reflect the collective affinity of microbes for a particular nutrient element. Therefore, the steady state cyanate concentrations in dark incubations may reflect balanced production and consumption of cyanate in incubations where organisms have a lesser affinity for cyanate utilization.

Urea, another N species recently found to support microbial nitrification (Alonso-Sáez et al., 2012; Connelly et al., 2014; Tolar et al., 2017; Widner et al., 2018a; Kitzinger et al., 2019; Kitzinger et al., 2020; Wan et al., 2021), behaved differently than cyanate in the dark bottle incubation experiments. The net production rate of urea was 0.15 μmol L^{-1} d^{-1} in the early linear phase while the net removal of urea was much faster, up to 0.35 μmol L^{-1} d^{-1} (Fig. 8c) suggesting that urea production limits its consumption and urea is one of the most preferred N substrates for nitrification in the Lafayette River. We know that urea is transported into microbial cells and decomposed by urease to NH_4^+ (see Figure 7.2 in Mulholland and Lomas, 2008). Among all examined N intermediates, urea was barely detectable in the water column even though substantial NH_4^+ accumulated at times (Figs. 4b & g and 5b & g), which suggests that the utilization of urea may be rapid and tightly coupled to its production. N+N concentrations rose after 10 days in dark incubations. While this is a rather long lag, and likely not representative of *in-situ* nitrification rates, it may indicate that there were few nitrifiers present in surface waters during sampling or that nitrifiers present were substrate limited until decay processes were underway. Because nitrifiers are usually not very abundant and active in euphotic surface waters due to

photoinhibition, it could have taken time for nitrifiers to become abundant enough to detect their activity in these concentration-based assays. Taken together, a further investigation of microbial community composition in the Lafayette River is needed.

In light incubations, concentrations of all N cycle intermediates, including cyanate, remained low throughout the degradation experiments suggesting that their production and uptake are tightly coupled in the euphotic zone (Figs. 8a-c), as has been observed previously for NH_4^+ and urea (Mulholland and Lomas, 2008). High cyanate concentrations during late spring and fall, when primary productivity and algal biomass were low suggests that cyanate is produced in the fall, as organic material decomposes and these high concentrations may persist through winter until organisms capable of their uptake emerge (e.g., Fig. 5f). In future studies, cyanate concentrations and uptake should be measured over the entire annual cycle to determine whether this is indeed the case.

4.2 Cyanate and nutrient release during wind-driven sediment resuspension events

Wind-driven sediment resuspension appears to be another external forcing that controls cyanate and other nitrogenous nutrient concentrations in the Lafayette River. High summertime productivity and settling of algal biomass transport a large pool of labile organic matter to the sediments that can be remineralized on short time scales (Schultz and Urban, 2008; Zhu et al., 2013). Regeneration of phytoplankton and other organic detritus in the sediments results in the reintroduction of nutrients to the water column through diffusive processes as well as advection, when there is a storm- or wind-induced sediment resuspension (Fong and Zedler, 2000; Yu et al., 2019). Sediment resuspension after storms and strong wind events resulted in increases in nutrient and Chl *a* concentrations during the days following (Filippino et al., 2017; Chen et al., 2018). McGill et al. (2019) showed that sediment resuspension in the Lafayette River can be induced and enhanced by elevated current speeds, and bottom wave orbital velocities >~2 cm s^{-1}, coinciding with wind speeds ≥5 m s^{-1}. For example, a large resuspension event caused by wind-generated waves occurred at AC on June 20, 2018 (storm 1, Fig. 4), when suspended sediment concentrations reached almost 6 g L^{-1} in the Lafayette River (McGill et al., 2019). Coincidently, this event was followed by an immediate increase in NH_4^+, N+N, and PO_4^{3-} concentrations, and a sharp decrease in Chl *a* concentrations (Figs. 4b-e & 4g-j); Chl *a* concentrations increased two or three days later, after the winds subsided and the storm had passed, in agreement with Morse et al. (2014).

Similar to the N compounds mentioned above, cyanate concentrations in bottom waters responded rapidly to the passage of storms, e.g., storms 1–5 in 2018 and 2019 (Figs. 4a & f, and 5a & f); concentrations increased by up to a factor of 3 as these storms passed through (Figs. 4a & f, 5a & f , and 6b & d), suggesting sediment resuspension is a major component of cyanate cycling in the shallow Lafayette River. Indeed, daily average wind speed and daily bottom cyanate concentrations were found to be significantly correlated for both years ($p<0.01$, *t*-test). Also, cross-correlations show the lag between daily average wind speed and daily bottom DIN concentrations was only 1 day (Fig. S5a, supporting information), whereas the lag between daily average wind speed and daily bottom cyanate concentrations was ~3 days (Fig. S5a, supporting information). Bottom cyanate and DIN concentrations were also shown to be positively correlated ($p<0.01$ for *t*-test) with lag of 1−2 days (Fig. S5b, supporting information). Cyanate was rapidly consumed, coincident with rising Chl *a* concentrations, suggesting that phytoplankton assemblages can utilize

cyanate to support their growth. The high cyanate concentrations in sediments during 2018 and dramatic increase in cyanate concentrations in response to wind-induced sediment resuspension suggests that remineralization of organic matter in the sediments is an important source of cyanate in shallow eutrophic estuaries.

5 Conclusions

To our knowledge, this is the first study examining the role of cyanate in the N cycle in an estuarine system. Cyanate concentrations varied from a few nmol L^{-1} to ~200 nmol L^{-1} in the Lafayette River, as for concentrations of other N cycle intermediates in summer, attesting to their lability. Bottom water cyanate concentrations were strongly correlated with storm-induced sediment resuspension suggesting that, like other N compounds, cyanate is produced in the sediments during organic matter remineralization. Degradation experiments confirmed that cyanate is also produced in the water column during organic matter decay. Further investigation of cyanate turnover times is needed to examine the importance of cyanate in primary production.

Acknowledgments

This study was funded by grants from the National Science Foundation (OCE-1459698), the Hampton Roads Sanitation District, and NOAA ECOHAB (NA18NOS4780176) to M.R.M. The authors sincerely thank Richard and Evelyn Reynolds, and Norfolk Yacht and Country Club (www.norfolkyacht.com) for their generosity and support in making their docks available for the sampling. We also wish to thank two anonymous reviewers for their careful reviews and helpful comments.

References

Alonso-Sáez, L., Waller, A.S., Mende, D.R., Bakker, K., Farnelid, H., Yager, P.L., Lovejoy, C., Tremblay, J.-É., Potvin, M., Heinrich, F., 2012. Role for urea in nitrification by polar marine Archaea. PNAS 109, 17989-17994.

Austin, J.A., 2002. Estimating the mean ocean-bay exchange rate of the Chesapeake Bay. J. Geophys. Res. Oceans 107, 131-138.

Babbin, A.R., Peters, B.D., Mordy, C.W., Widner, B., Casciotti, K.L., Ward, B.B., 2017. Multiple metabolisms constrain the anaerobic nitrite budget in the Eastern Tropical South Pacific. Glob. Biogeochem. Cycles 31, 258-271.

Bayer, B., Saito, M.A., McIlvin, M.R., Lücker, S., Moran, D.M., Lankiewicz, T.S., Dupont, C.L., Santoro, A.E., 2021. Metabolic versatility of the nitrite-oxidizing bacterium Nitrospira marina and its proteomic response to oxygen-limited conditions. ISME J. 15, 1025-1039.

Berg, G.M., Balode, M., Purina, I., Bekere, S., Béchemin, C., Maestrini, S.Y., 2003. Plankton community composition in relation to availability and uptake of oxidized and reduced nitrogen. Aquat. Microb. Ecol. 30, 263-274.

Berg, G.M., Shrager, J., Glöckner, G., Arrigo, K.R., Grossman, A.R., 2008. Understanding nitrogen limitation in Aureococcus Anophagefferens (Pelagophyceae) through cDNA and qRT-QPCR analysis. J. Phycol. 44, 1235-1249.

Bernhardt, H., Wilhelms, A., 1967. The continuous determination of low level iron, soluble phosphate and total phosphate with the AutoAnalyzer, Technicon symposia, pp. 385-389.

Bronk, D., See, J., Bradley, P., Killberg, L., 2007. DON as a source of bioavailable nitrogen for phytoplankton. Biogeosciences 4, 283-296.

Burdige, D.J., Zheng, S., 1998. The biogeochemical cycling of dissolved organic nitrogen in estuarine sediments. Limnol. Oceanogr. 43, 1796-1813.

Chen, N., Mo, Q., Kuo, Y.-M., Su, Y., Zhong, Y., 2018. Hydrochemical controls on reservoir nutrient and phytoplankton dynamics under storms. Sci. Total Environ. 619, 301-310.

Collos, Y., Jauzein, C., Ratmaya, W., Souchu, P., Abadie, E., Vaquer, A., 2014. Comparing diatom and Alexandrium catenella/tamarense blooms in Thau lagoon: Importance of dissolved organic nitrogen in seasonally N-limited systems. Harmful Algae 37, 84-91.

Connelly, T.L., Baer, S.E., Cooper, J.T., Bronk, D.A., Wawrik, B., 2014. Urea uptake and carbon fixation by marine pelagic bacteria and archaea during the Arctic summer and winter seasons. Appl. Environ. Microbiol. 80, 6013-6022.
Cowan, J.L., Boynton, W.R., 1996. Sediment-water oxygen and nutrient exchanges along the longitudinal axis of Chesapeake Bay: seasonal patterns, controlling factors and ecological significance. Estuaries 19, 562-580.
Davidson, K., Gowen, R.J., Tett, P., Bresnan, E., Harrison, P.J., McKinney, A., Milligan, S., Mills, D.K., Silke, J., Crooks, A.-M., 2012. Harmful algal blooms: how strong is the evidence that nutrient ratios and forms influence their occurrence? Estuar. Coast. Shelf Sci. 115, 399-413.
Egerton, T., Morse, R., Marshall, H., Mulholland, M., 2014. Emergence of algal blooms: the effects of short-term variability in water quality on phytoplankton abundance, diversity, and community composition in a tidal estuary. Microorganisms 2, 33-57.
Elferink, S., John, U., Neuhaus, S., Wohlrab, S., 2020. Functional genomics differentiate inherent and environmentally influenced traits in dinoflagellate and diatom communities. Microorganisms 8, 567.
Filippino, K.C., Egerton, T.A., Hunley, W.S., Mulholland, M.R., 2017. The influence of storms on water quality and phytoplankton dynamics in the tidal James River. Estuaries Coasts 40, 80-94.
Fong, P., Zedler, J.B., 2000. Sources, sinks, and fluxes of nutrients (N + P) in a small highly modified urban estuary in southern California. Urban Ecosyst. 4, 125-144.
Ganesh, S., Bertagnolli, A.D., Bristow, L.A., Padilla, C.C., Blackwood, N., Aldunate, M., Bourbonnais, A., Altabet, M.A., Malmstrom, R.R., Woyke, T., 2018. Single cell genomic and transcriptomic evidence for the use of alternative nitrogen substrates by anammox bacteria. ISME J. 12, 2706-2722.
Glibert, P.M., Burkholder, J.M., 2011. Harmful algal blooms and eutrophication:“strategies” for nutrient uptake and growth outside the Redfield comfort zone. Chin. J. Oceanol. Limnol. 29, 724-738.
Glibert, P.M., Legrand, C., 2006. The diverse nutrient strategies of harmful algae: focus on osmotrophy, in: Granéli, E., Turner, J.T. (Eds.), Ecology of harmful algae. Springer, Berlin, Heidelberg, pp. 163-175.
Glibert, P.M., Magnien, R., Lomas, M.W., Alexander, J., Tan, C., Haramoto, E., Trice, M., Kana, T.M., 2001. Harmful algal blooms in the Chesapeake and coastal bays of Maryland, USA: comparison of 1997, 1998, and 1999 events. Estuaries 24, 875-883.
Gobler, C.J., Burson, A., Koch, F., Tang, Y., Mulholland, M.R., 2012. The role of nitrogenous nutrients in the occurrence of harmful algal blooms caused by Cochlodinium polykrikoides in New York estuaries (USA). Harmful Algae 17, 64-74.
Hagy, J.D., Boynton, W.R., Keefe, C.W., Wood, K.V., 2004. Hypoxia in Chesapeake Bay, 1950–2001: long-term change in relation to nutrient loading and river flow. Estuaries 27, 634-658.
Harding, L.W., Adolf, J., Mallonee, M., Miller, W., Gallegos, C.L., Perry, E., Johnson, J., Sellner, K., Paerl, H., 2015. Climate effects on phytoplankton floral composition in Chesapeake Bay. Estuar. Coast. Shelf Sci. 162, 53-68.
Harding, L.W., Mallonee, M.E., Perry, E.S., Miller, W.D., Adolf, J.E., Gallegos, C.L., Paerl, H.W., 2016. Variable climatic conditions dominate recent phytoplankton dynamics in Chesapeake Bay. Sci. Rep. 6, 1-16.
Harding, L.W., Mallonee, M.E., Perry, E.S., Miller, W.D., Adolf, J.E., Gallegos, C.L., Paerl, H.W., 2019. Long-term trends, current status, and transitions of water quality in Chesapeake Bay. Sci. Rep. 9, 1-19.
Hofmann, E.E., Klinck, J.M., Filippino, K.C., Egerton, T., Davis, L.B., Echevarría, M., Pérez-Vega, E., Mulholland, M.R., 2021. Understanding controls on Margalefidinium polykrikoides blooms in the lower Chesapeake Bay. Harmful Algae 107, 102064.
Hu, Z., Mulholland, M.R., Duan, S., Xu, N., 2012. Effects of nitrogen supply and its composition on the growth of Prorocentrum donghaiense. Harmful Algae 13, 72-82.
Kamennaya, N.A., Chernihovsky, M., Post, A.F., 2008. The cyanate utilization capacity of marine unicellular Cyanobacteria. Limnol. Oceanogr. 53, 2485-2494.
Kamennaya, N.A., Post, A.F., 2011. Characterization of cyanate metabolism in marine Synechococcus and Prochlorococcus spp. Appl. Environ. Microbiol. 77, 291-301.
Kamennaya, N.A., Post, A.F., 2013. Distribution and expression of the cyanate acquisition potential among cyanobacterial populations in oligotrophic marine waters. Limnol. Oceanogr. 58, 1959-1971.
Kitzinger, K., Marchant, H.K., Bristow, L.A., Herbold, C.W., Padilla, C.C., Kidane, A.T., Littmann, S., Daims, H., Pjevac, P., Stewart, F.J., 2020. Single cell analyses reveal contrasting life strategies of the two main nitrifiers in the ocean. Nat. Commun. 11, 1-12.
Kitzinger, K., Padilla, C.C., Marchant, H.K., Hach, P.F., Herbold, C.W., Kidane, A.T., Könneke, M., Littmann, S., Mooshammer, M., Niggemann, J., 2019. Cyanate and urea are substrates for nitrification by Thaumarchaeota in the marine environment. Nat. Microbiol 4, 234-243.

Koch, H., van Kessel, M.A., Lücker, S., 2019. Complete nitrification: insights into the ecophysiology of comammox Nitrospira. Appl. Microbiol. Biotechnol. 103, 177-189.
Lücker, S., Wagner, M., Maixner, F., Pelletier, E., Koch, H., Vacherie, B., Rattei, T., Damsté, J.S.S., Spieck, E., Le Paslier, D., 2010. A Nitrospira metagenome illuminates the physiology and evolution of globally important nitrite-oxidizing bacteria. PNAS 107, 13479-13484.
Marshall, H.G., Egerton, T.A., 2009. Phytoplankton blooms: Their occurrence and composition within Virginia's tidal tributaries. Va. j. sci. 60, 3.
Martins, C.G., Cross, J., 2022. TEOS-10 Excel–implementation of the Thermodynamic Equation Of Seawater–2010 in Excel. Ocean Sci. 18, 627-638.
McGill, S.C., Hale, R.P., Mulholland, M.R., 2019. Sediment Resuspension in a Microtidal Estuary: Causative Forces and Links with Algal Blooms. Master of Science (MS), Thesis, Ocean, Earth & Atomspheric Sciences, Old Dominion University.
Miller, A.G., Espie, G.S., 1994. Photosynthetic metabolism of cyanate by the cyanobacterium Synechococcus UTEX 625. Arch. Microbiol. 162, 151-157.
Mooshammer, M., Wanek, W., Jones, S.H., Richter, A., Wagner, M., 2021. Cyanate is a low abundance but actively cycled nitrogen compound in soil. Commun. Earth Environ. 2, 1-10.
Morse, R.E., Mulholland, M.R., Egerton, T.A., Marshall, H.G., 2014. Phytoplankton and nutrient dynamics in a tidally dominated eutrophic estuary: daily variability and controls on bloom formation. Mar. Ecol. Prog. Ser. 503, 59-74.
Morse, R.E., Mulholland, M.R., Hunley, W.S., Fentress, S., Wiggins, M., Blanco-Garcia, J.L., 2013. Controls on the initiation and development of blooms of the dinoflagellate Cochlodinium polykrikoides Margalef in lower Chesapeake Bay and its tributaries. Harmful Algae 28, 71-82.
Morse, R.E., Shen, J., Blanco-Garcia, J.L., Hunley, W.S., Fentress, S., Wiggins, M., Mulholland, M.R., 2011. Environmental and physical controls on the formation and transport of blooms of the dinoflagellate Cochlodinium polykrikoides Margalef in the lower Chesapeake Bay and its tributaries. Estuaries Coasts 34, 1006-1025.
Moschonas, G., Gowen, R.J., Paterson, R.F., Mitchell, E., Stewart, B.M., McNeill, S., Glibert, P.M., Davidson, K., 2017. Nitrogen dynamics and phytoplankton community structure: the role of organic nutrients. Biogeochemistry 134, 125-145.
Mulholland, M.R., Gobler, C.J., Lee, C., 2002. Peptide hydrolysis, amino acid oxidation, and nitrogen uptake in communities seasonally dominated by Aureococcus anophagefferens. Limnol. Oceanogr. 47, 1094-1108.
Mulholland, M.R., Lomas, M.W., 2008. Nitrogen uptake and assimilation, in: Capone, D.G., Bronk, D.A., Mulholland, M.R., Carpenter, E.J. (Eds.), Nitrogen in the marine environment, 2nd ed. Academic Press, pp. 303-384.
Mulholland, M.R., Morse, R., Egerton, T., Bernhardt, P.W., Filippino, K., 2018. Blooms of dinoflagellate mixotrophs in a lower Chesapeake Bay tributary: carbon and nitrogen uptake over diurnal, seasonal, and interannual timescales. Estuaries Coasts 41, 1744-1765.
Mulholland, M.R., Morse, R.E., Boneillo, G.E., Bernhardt, P.W., Filippino, K.C., Procise, L.A., Blanco-Garcia, J.L., Marshall, H.G., Egerton, T.A., Hunley, W.S., 2009. Understanding causes and impacts of the dinoflagellate, Cochlodinium polykrikoides, blooms in the Chesapeake Bay. Estuaries Coasts 32, 734-747.
Pachiadaki, M.G., Sintes, E., Bergauer, K., Brown, J.M., Record, N.R., Swan, B.K., Mathyer, M.E., Hallam, S.J., Lopez-Garcia, P., Takaki, Y., 2017. Major role of nitrite-oxidizing bacteria in dark ocean carbon fixation. Science 358, 1046-1051.
Palatinszky, M., Herbold, C., Jehmlich, N., Pogoda, M., Han, P., von Bergen, M., Lagkouvardos, I., Karst, S.M., Galushko, A., Koch, H., 2015. Cyanate as an energy source for nitrifiers. Nature 524, 105.
Palenik, B., Brahamsha, B., Larimer, F., Land, M., Hauser, L., Chain, P., Lamerdin, J., Regala, W., Allen, E., McCarren, J., 2003. The genome of a motile marine Synechococcus. Nature 424, 1037.
Park, J.G., Jeong, M.K., Lee, J.A., Cho, K.-J., Kwon, O.-S., 2001. Diurnal vertical migration of a harmful dinoflagellate, Cochlodinium polykrikoides (Dinophyceae), during a red tide in coastal waters of Namhae Island, Korea. Phycologia 40, 292-297.
Rahmatullah, M., Boyde, T., 1980. Improvements in the determination of urea using diacetyl monoxime; methods with and without deproteinisation. Clin. Chim. Acta 107, 3-9.
Rocap, G., Larimer, F.W., Lamerdin, J., Malfatti, S., Chain, P., Ahlgren, N.A., Arellano, A., Coleman, M., Hauser, L., Hess, W.R., Johnson, Z.I., Land, M., Lindell, D., Post, A.F., Regala, W., Shah, M., Shaw, S.L., Steglich, C., Sullivan, M.B., Ting, C.S., Tolonen, A., Webb, E.A., Zinser, E.R., Chisholm, S.W., 2003. Genome divergence in two Prochlorococcus ecotypes reflects oceanic niche differentiation. Nature 424, 1042-1047.

718 Schultz, P., Urban, N.R., 2008. Effects of bacterial dynamics on organic matter decomposition and nutrient release
719 from sediments: A modeling study. Ecol. Modell. 210, 1-14.
720 Sima, W., Hu, M., He, Q., Qiu, Y., Lv, Y., Dai, L., Shao, Q., Zhou, T., Li, H., Zhou, M., 2020. Regulation of
721 nitrogen dynamics at the sediment–water interface during HAB degradation and subsequent reoccurrence. RSC Adv.
722 10, 13480-13488.
723 Strickland, J.D., Parsons, T.R., 1972. A practical handbook of seawater analysis, 2nd ed. Fisheries Research Board
724 of Canada, Ottawa.
725 Tang, T., Filippino, K.C., Liu, Z., Mulholland, M.R., Lee, C., 2017. Peptide hydrolysis and uptake of peptide
726 hydrolysis products in the James River estuary and lower Chesapeake Bay. Mar. Chem. 197, 52-63.
727 Testa, J.M., Murphy, R.R., Brady, D.C., Kemp, W.M., 2018. Nutrient-and climate-induced shifts in the phenology
728 of linked biogeochemical cycles in a temperate estuary. Front. Mar. Sci. 5, 114.
729 Tolar, B.B., Wallsgrove, N.J., Popp, B.N., Hollibaugh, J.T., 2017. Oxidation of urea-derived nitrogen by
730 thaumarchaeota-dominated marine nitrifying communities. Environ. Microbiol. 19, 4838-4850.
731 Wan, X.S., Sheng, H.X., Dai, M., Church, M.J., Zou, W., Li, X., Hutchins, D.A., Ward, B.B., Kao, S.J., 2021.
732 Phytoplankton-Nitrifier Interactions Control the Geographic Distribution of Nitrite in the Upper Ocean. Global
733 Biogeochem Cycles 35, e2021GB007072.
734 Welschmeyer, N.A., 1994. Fluorometric analysis of chlorophyll a in the presence of chlorophyll b and
735 pheopigments. Limnol. Oceanogr. 39, 1985-1992.
736 Whitledge, T.E., Malloy, S., Patton, C.J., Wirick, C.D., 1981. Automated nutrient analyses in seawater. Brookhaven
737 National Lab., Upton, NY (USA).
738 Widner, B., Fuchsman, C.A., Chang, B.X., Rocap, G., Mulholland, M.R., 2018a. Utilization of urea and cyanate in
739 waters overlying and within the eastern tropical north Pacific oxygen deficient zone. FEMS Microbiol. Ecol. 94,
740 fiy138.
741 Widner, B., Mordy, C.W., Mulholland, M.R., 2018b. Cyanate distribution and uptake above and within the Eastern
742 Tropical South Pacific oxygen deficient zone. Limnol. Oceanogr. 63, S177-S192.
743 Widner, B., Mulholland, M.R., 2017. Cyanate distribution and uptake in North Atlantic coastal waters. Limnol.
744 Oceanogr. 62, 2538-2549.
745 Widner, B., Mulholland, M.R., Mopper, K., 2013. Chromatographic determination of nanomolar cyanate
746 concentrations in estuarine and sea waters by precolumn fluorescence derivatization. Anal. Chem. 85, 6661-6666.
747 Widner, B., Mulholland, M.R., Mopper, K., 2016. Distribution, sources, and sinks of cyanate in the coastal North
748 Atlantic Ocean. Environ. Sci. Technol. Lett. 3, 297-302.
749 Wu, K., Lu, K., Dai, M., Liu, Z., 2019. The bioavailability of riverine dissolved organic matter in coastal marine
750 waters of southern Texas. Estuar. Coast. Shelf Sci. 231, 106477.
751 Yu, D., Chen, N., Krom, M.D., Lin, J., Cheng, P., Yu, F., Guo, W., Hong, H., Gao, X., 2019. Understanding how
752 estuarine hydrology controls ammonium and other inorganic nitrogen concentrations and fluxes through the
753 subtropical Jiulong River Estuary, SE China under baseflow and flood-affected conditions. Biogeochemistry 142,
754 443-466.
755 Zhang, Q., Brady, D.C., Boynton, W.R., Ball, W.P., 2015. Long-term trends of nutrients and sediment from the
756 nontidal Chesapeake watershed: An assessment of progress by river and season. JAWRA 51, 1534-1555.
757 Zhu, M., Zhu, G., Zhao, L., Yao, X., Zhang, Y., Gao, G., Qin, B., 2013. Influence of algal bloom degradation on
758 nutrient release at the sediment–water interface in Lake Taihu, China. Environ. Sci. Pollut. Res. 20, 1803-1811.
759 Zhuang, Y., Zhang, H., Hannick, L., Lin, S., 2015. Metatranscriptome profiling reveals versatile N-nutrient
760 utilization, CO2 limitation, oxidative stress, and active toxin production in an Alexandrium fundyense bloom.
761 Harmful Algae 42, 60-70.
762

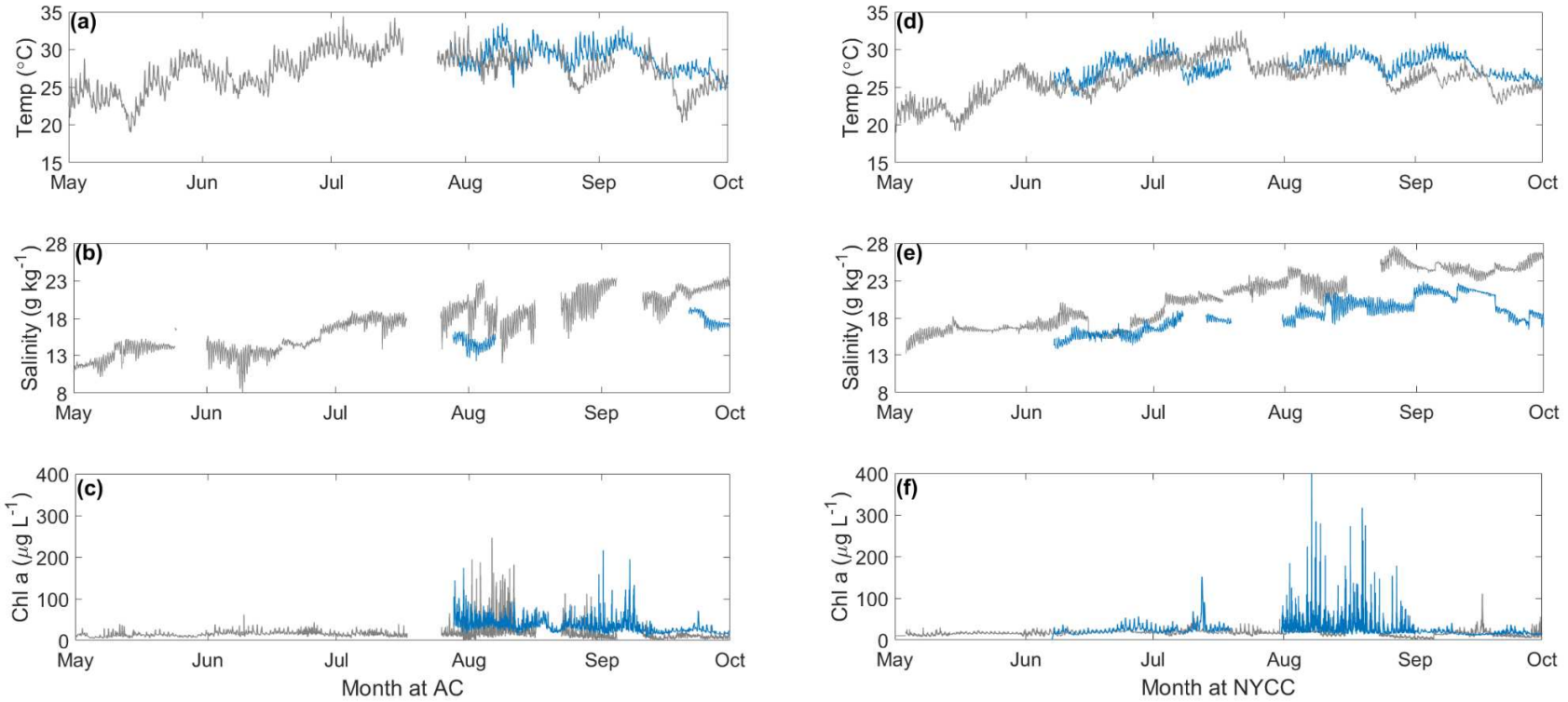

Figure 1. Time-series data from YSI data sondes deployed at stations AC (left panels) and NYCC (right panels). Data collected include temperature (panels a & d), absolute salinity (panels b & e), and Chl *a* (panels c & f) in summer 2018 (blue line) and 2019 (gray line).

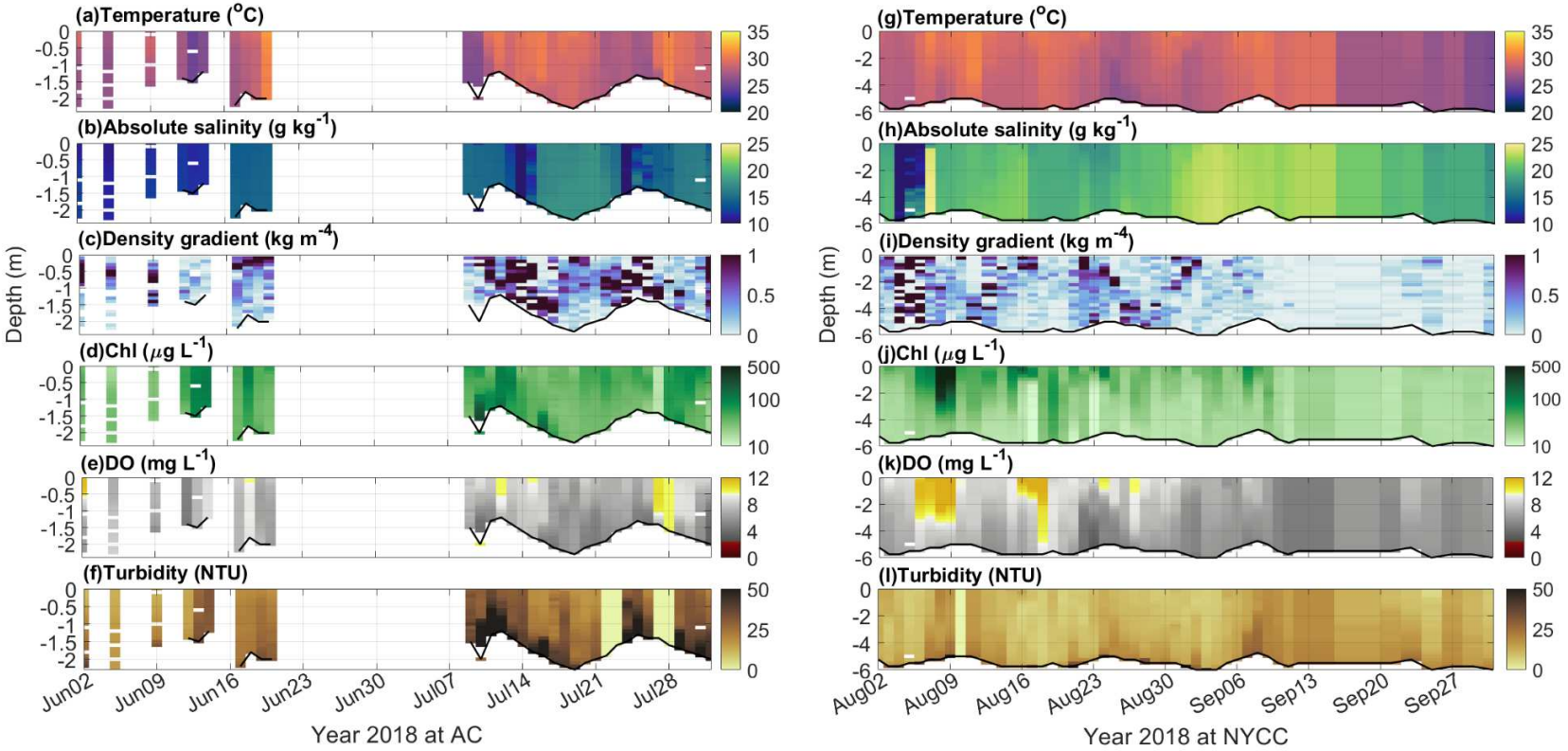

Figure 2. Time-series data collected at stations AC (left panels, 0.1 m binned) and NYCC (right panels, 0.25 m binned) in the Lafayette River using YSI data sondes that include measurements of temperature (panels a & g), absolute salinity (panels b & h), density gradient (panels c & i), Chl *a* (panels d & j), DO (panels e & k) and turbidity (panels f & l; NTU: nephelometric turbidity units) in summer 2018. Note the colorbars of Chl *a* were shown in log scale.

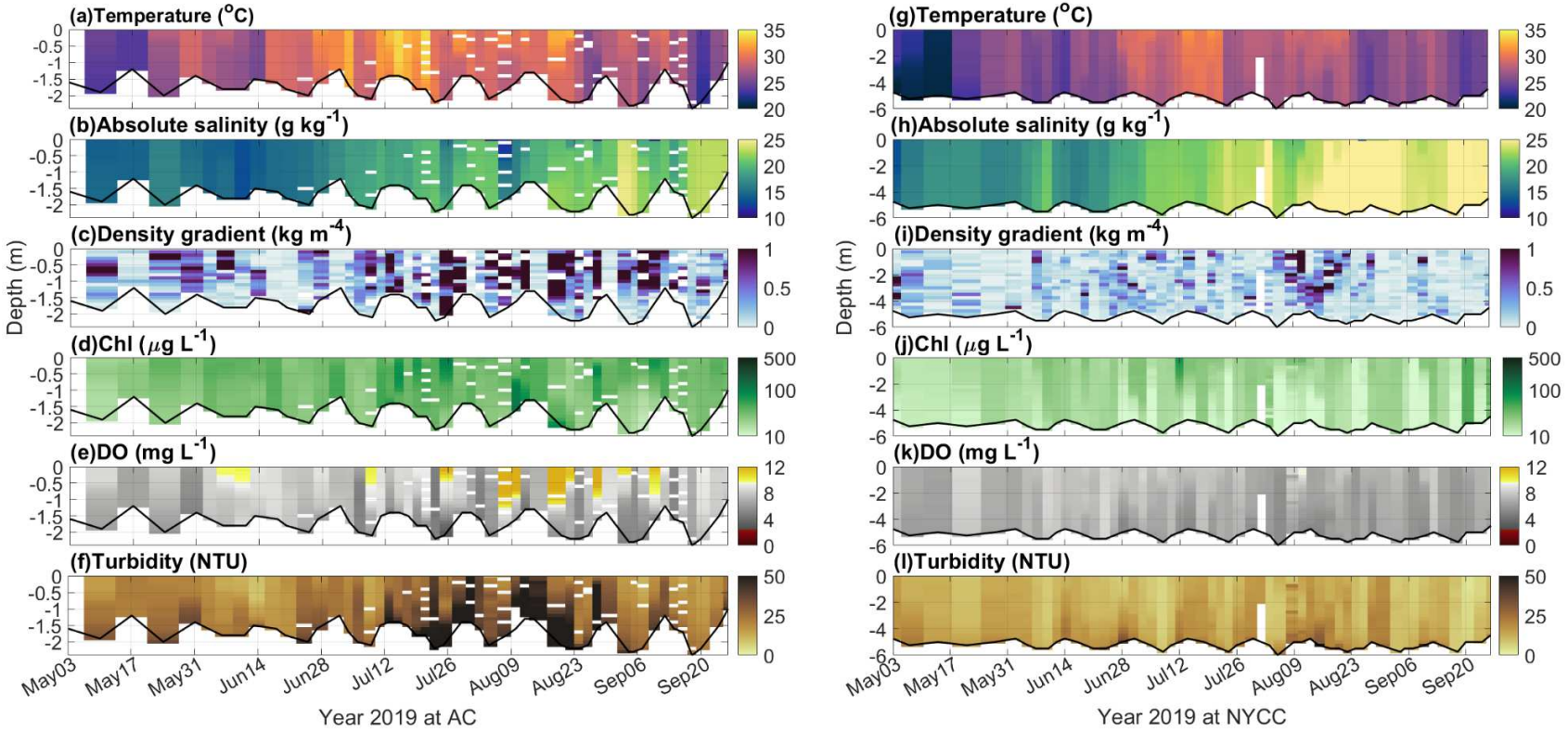

Figure 3. Time-series data collected at stations AC (left panels, 0.1 m binned) and NYCC (right panels, 0.25 m binned) in the Lafayette River using YSI data sondes that include measurements of temperature (panels a & g), absolute salinity (panels b & h), density gradient (panels c & i), Chl *a* (panels d & j), DO (panels e & k), and turbidity (panels f & l) in summer 2019. Note the colorbars of Chl *a* were shown in log scale.

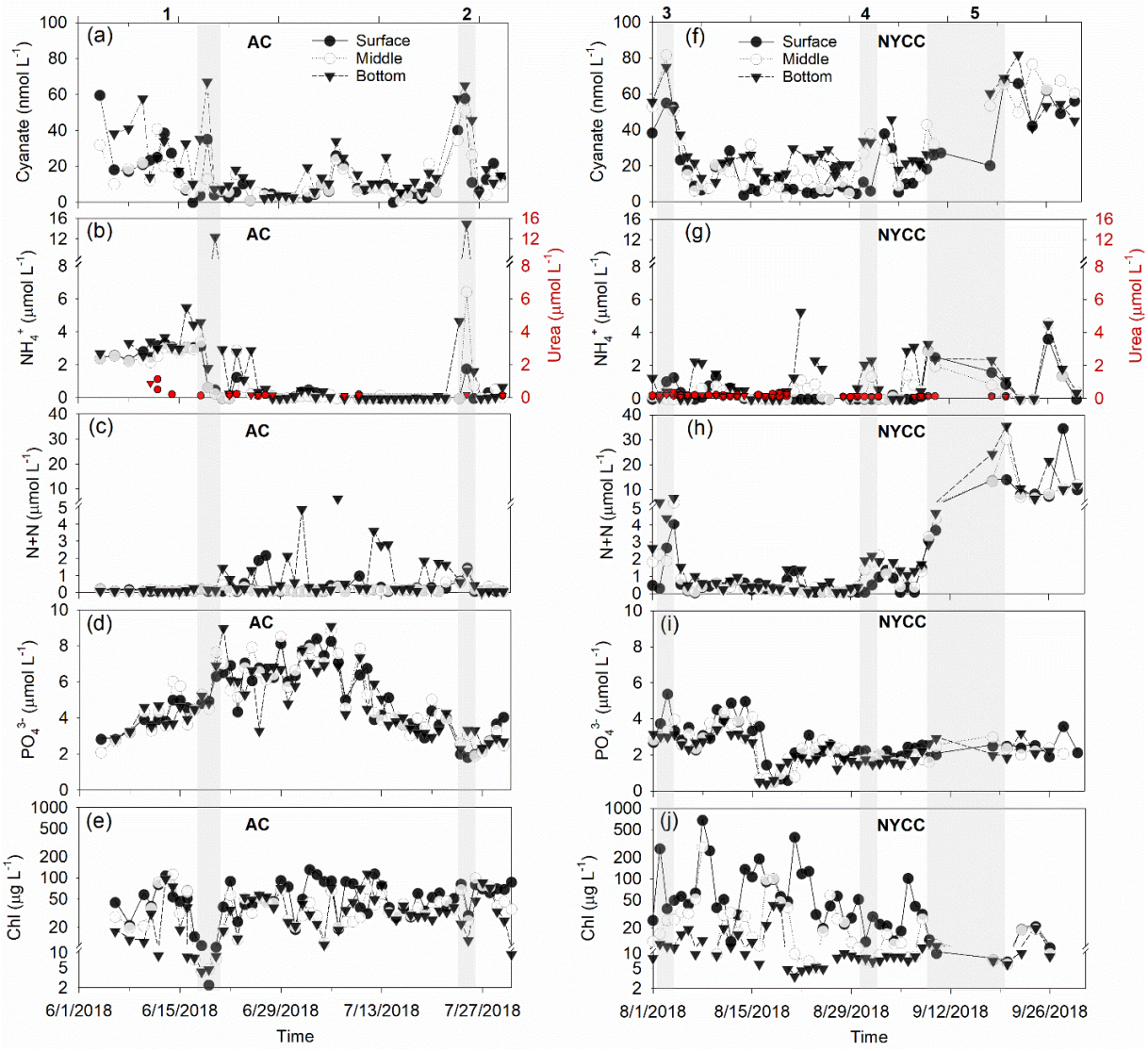

Figure 4. Time series data of cyanate (a & f), NH_4^+ and urea (b & g), N+N (nitrate+ nitrite, c & h), PO_4^{3-} (d & i), and extracted Chl *a* (e & j) collected from near-surface (black circles), at mid-depth (white circles), and near-bottom (black triangles) at stations AC (June 1–July 30, 2018) and NYCC (August 1–October 1, 2018). Red dots represent urea concentration. Gray shading indicates passage of major storms 1–5 during the sampling period in 2018. Storm 5 was hurricane Florence which occurred during September 12–16, 2018.

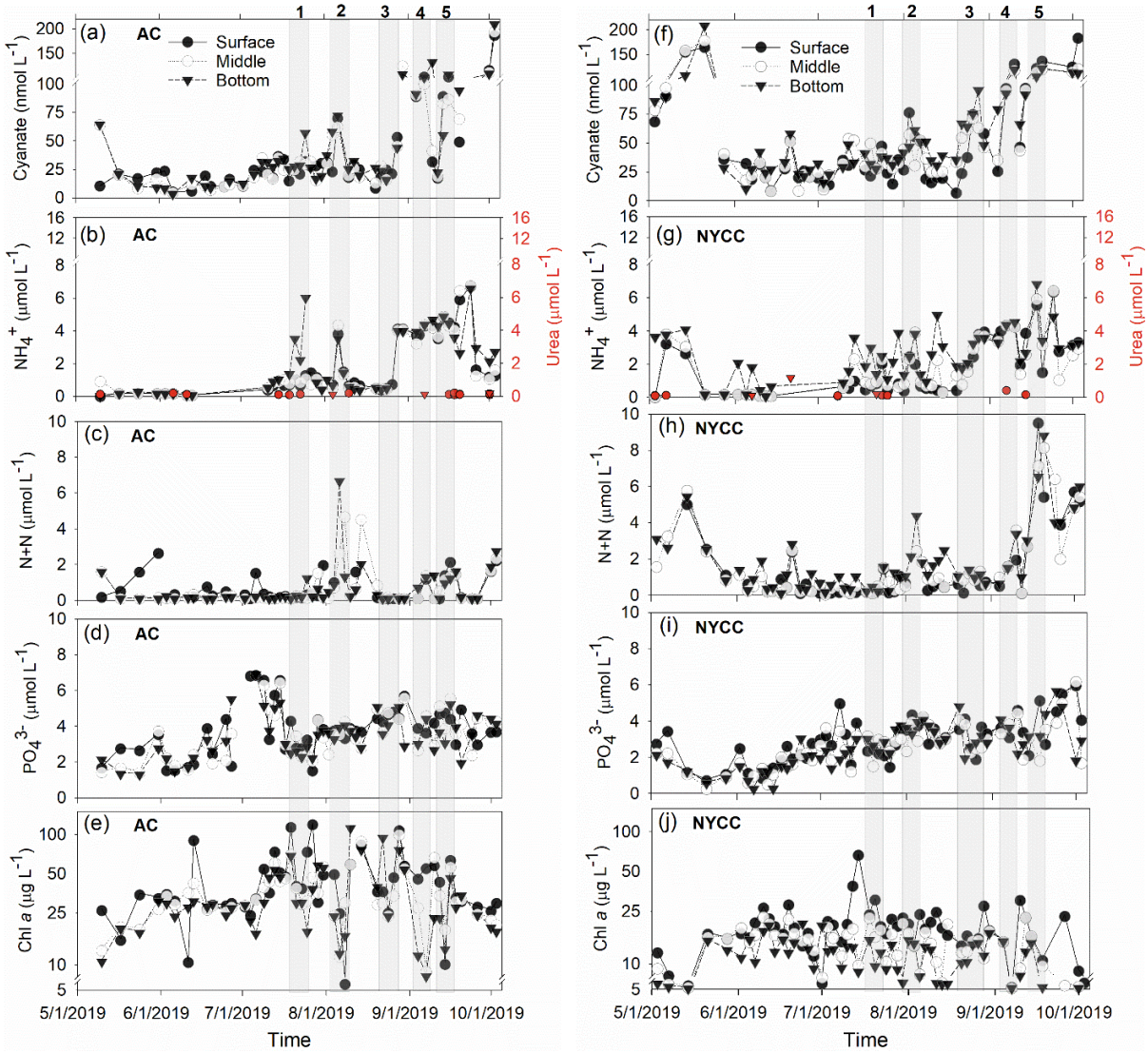

Figure 5. Time series data of cyanate (a & f), NH_4^+ and urea (b & g), N+N (nitrate+ nitrite, c & h), PO_4^{3-} (d & i), and extracted Chl *a* (e & j) collected from near-surface (black circles), at mid-depth (white circles), and near-bottom (black triangles) at stations AC (left panels) and NYCC (right panels) from May 1 to October 1, 2019. Red dots represent urea concentration. Gray shading indicates passage of major storms 1–5 during the sampling period in 2019. Storm 4 was hurricane Dorian which occurred during September 5–6, 2019.

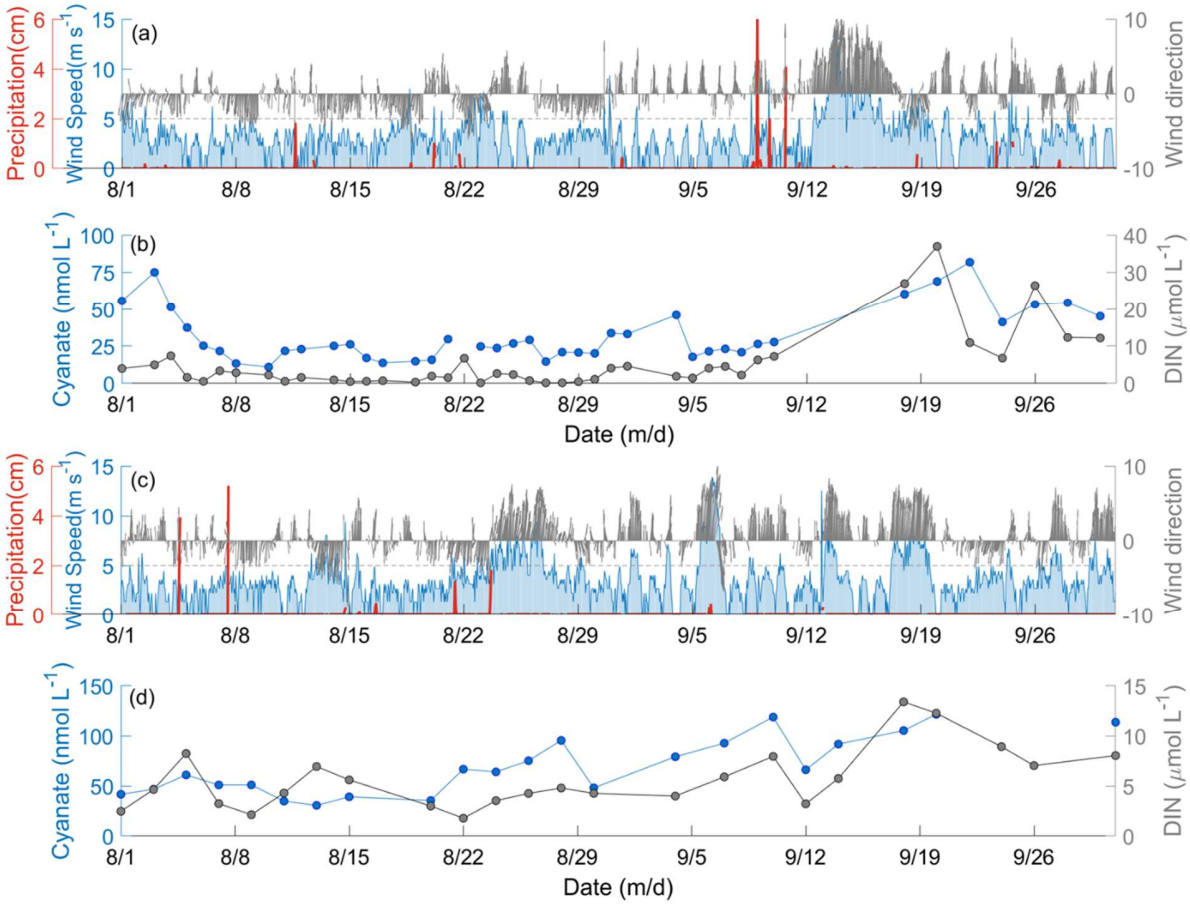

Figure 6. (a) wind speed (blue shaded lines), wind direction (gray vectors, negative indicates winds were from the south), and precipitation (red lines) at Norfolk Naval Station (station ID: 13750, [36.95°N, -76.30°E]), and (b) observed bottom cyanate concentrations (blue dots) and DIN (the sum of NH_4^+ and N+N, gray dots) at NYCC in August and September 2018; (c) and (d) are the same as (a) and (b) but for 2019. Gray dashed line in (a) and (c) indicates the threshold of storm with wind speed of 5 m s^{-1}. Wind data were obtained from https://www.ncdc.noaa.gov/cdo-web/datatools/lcd.

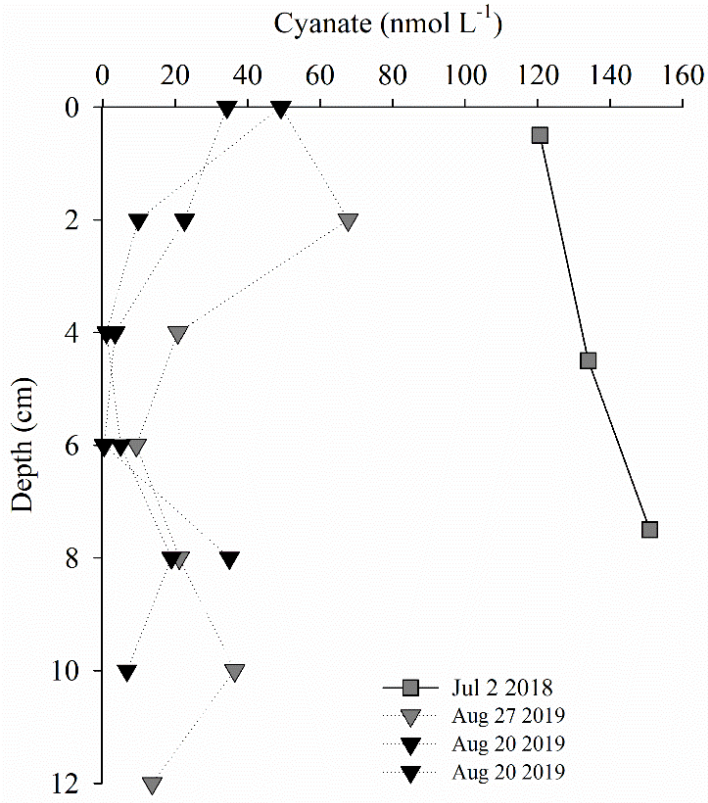

Figure 7. Cyanate profiles from sediment cores collected at AC on July 2, 2018, and August 20 and 27, 2019.

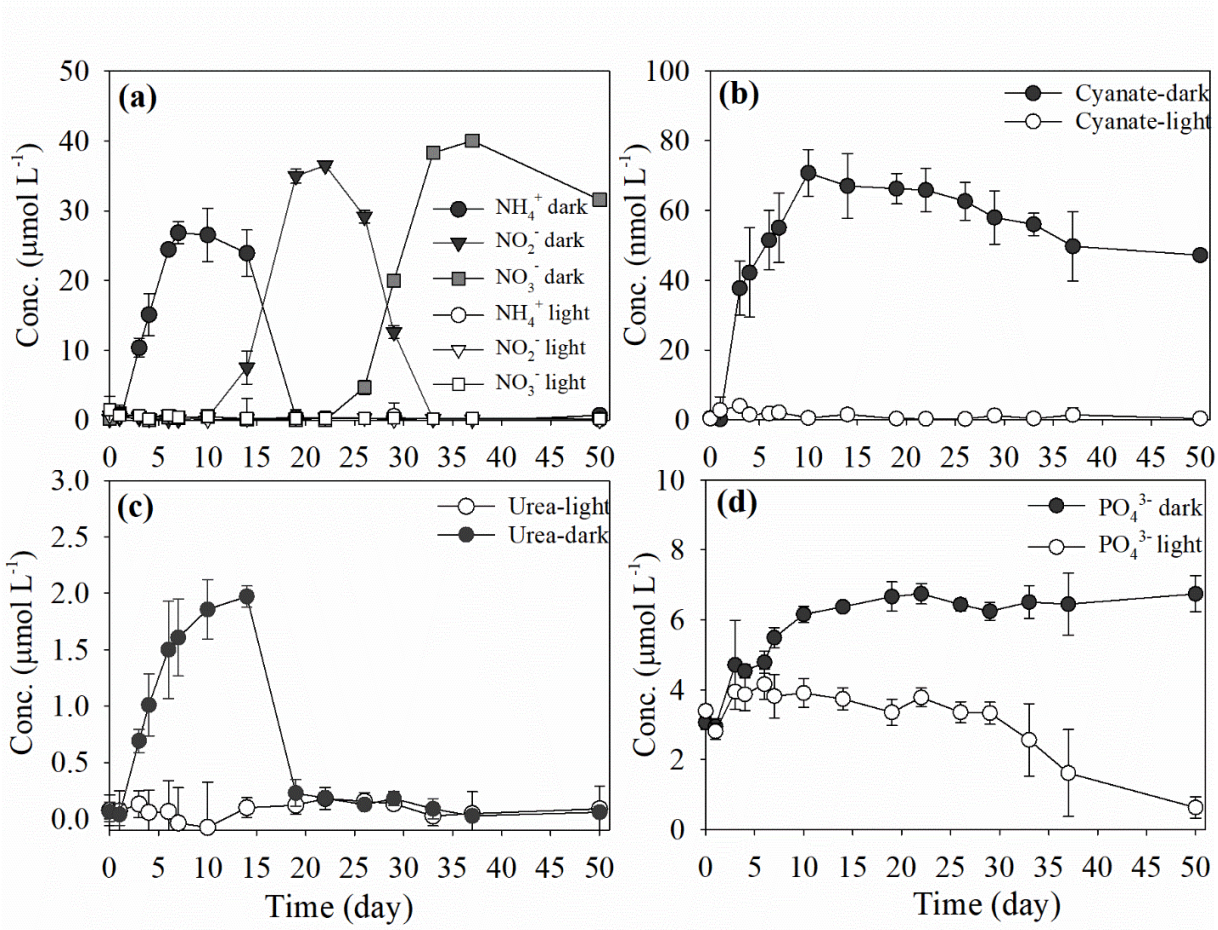

Figure 8. Results from degradation experiments using natural water collected during a bloom of *Margalefidinium polykrikoides* in August 2018, showing the variations in (a) NH_4^+, NO_2^-, and NO_3^-, (b) cyanate, (c) urea, and (d) PO_4^{3-} concentrations over the 50-day incubation period in the dark (dark markers) and light (white markers).